ACS OMEGA

http://pubs.acs.org/journal/acsodf

Article

Study on the Movement of Pulverized Coal Particles in Fractal Fracture Network

Songlei Tang,* Qiang Liu, Hong Tang, and Feng Yang

Cite This: *ACS Omega* 2023, 8, 26369−26378

Read Online

ACCESS | Metrics & More | Article Recommendations

ABSTRACT: Coalbed methane (CBM) exploitation is a complex multiphase flow process. With the development of CBM extraction technology, it is recognized that the migration of reservoir fluid in the fracture network is affected by the matrix fracture structure, fracture width, and pulverized coal particles plugging, therefore the fluid-particle coupling problem has received increasing attention. In this paper, six groups of fracture models with different fractal dimensions are established using the Weierstrass−Mandelbrot function, and the fluid-particle coupling phenomena in fractures with different roughness and aperture are simulated using an immersed boundary-lattice Boltzmann method (IB-LBM), by comparing the numerical simulation results with the theoretical analysis, it is proved that the IB-LBM numerical method has high accuracy and effectiveness. The effects of fractal dimension, particle size, and particle concentration on the plugging effect were investigated. The results show that the plugging effect on the fracture is enhanced with the increase of the pulverized coal particles content. When the concentration and size of pulverized coal particles are the same, the migration path of pulverized coal particles in complex fractures is more tortuous and more likely to be plugged. It may lead to a shift in the main seepage network of the fracture and the formation of new seepage channels. The research in this paper provides a data basis for the formation and plugging pattern of pulverized coal particles in coal seam fractures, which can provide a basis for the control of pulverized coal particles concentration in CBM drainage.

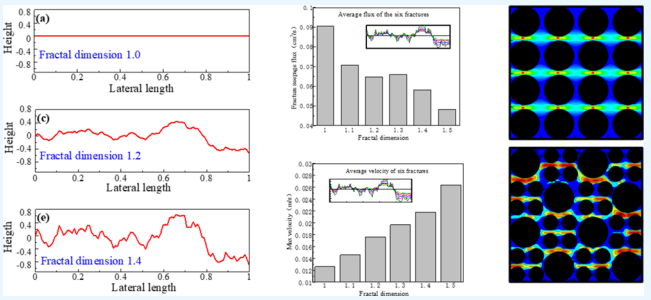

1. INTRODUCTION

Compared to conventional rock media, the structure of the coal matrix is mostly anisotropic.[1] Due to the complex occurrence environment and numerous fault structures, the cementation of the coal matrix is weak.[2] The complex fracture network characteristics of the coal matrix led to the generation of pulverized coal particles in the fractures. Meanwhile, the strong scouring effect of fracturing fluid on the coal matrix after fracturing can cause coal fragmentation. Pulverized coal particles blockage has become the most serious reservoir damage mode in CBM extraction.[3] The migration and plugging effects of pulverized coal particles have caused serious hazards to the stable development of CBM drainage wells.[4]

The damage of pulverized coal particles on the permeability of coal seams is manifested in the following aspects. First, the pulverized coal particles are easily captured by the fine pore space, and the captured pulverized coal particles tend to block the originally connected pores of the coal seam, increasing the length of the moving path, and thus reducing the permeability of the coal seam.[5] Second, a large amount of proppant particles are injected during the fracturing process. During this process, fine coal particles tend to invade the pore space, mix with the proppant, and adhere to the pore space, thus reducing the conductivity of the proppant package.[6] In addition, pulverized coal particles that are not captured by the formation tend to invade the wellbore, and long-term accumulation and retention can lead to accidents, such as pump jams and pump burial, and may even block the main pipeline of CBM production.[7] Pulverized coal particles are harmful to the safety of coalbed methane production in many ways, greatly increase the development cost of CBM reservoir, and cause production reduction accidents.

Pulverized coal particles tend to accumulate in the flow channels, and the accumulated pulverized coal particles tend to block the network structure of coal rock fractures.[8] Bedrikovetsky et al.[9−11] have pointed out that slip is the main reason for the generation of pulverized coal particles. The fluid channels in fractures are irregular and when the fluid passes through the seepage channel, the frictional impact on the fracture wall is high due to the excessive flow rate, and the coal

Received: April 27, 2023
Accepted: June 28, 2023
Published: July 16, 2023

matrix is strongly impacted, resulting in the formation of a large number of pulverized coal particles.

The main reason for the generation of pulverized coal particles is that during the drainage and decompression process, the drainage speed is too fast, resulting in the impact of water on the soft coal matrix, which exceeds the maximum shear strength that the coal matrix can withstand. As a result, a large number of pulverized coal particles were generated in the coal matrix. In 2016 and 2018, Wei et al.[12,13] investigated the main factors affecting the yield of pulverized coal particles. Their study attributed the main factor of coal dust particle production to the tensile damage of the coal matrix. They concluded that the high-pressure effect of hydraulic fracturing resulted in the production of large amounts of pulverized coal particles and that excessive pressure variations should be reduced during the production process. Xu et al.[14] realized that the difference in the properties of clay minerals was also the major factor affecting the yield of pulverized coal particles. They pointed out that if the coal matrix contains high content of kaolinite and illite, more pulverized coal particles will be produced.

In the characterization of porous media in coal rocks, Payatakes and Reddi et al.[15,16] were the first to propose an ideal capillary model for quantitative analysis and characterization of porous media structures. In this capillary model, the porous media reduced to many capillary bundles, while the pore space is idealized. Happel[17] proposed a spherical porous media model, which considers porous media as microelements composed of spheres of different diameters. Bandis et al.[18] concluded that the geometric and strength characteristics of roughness on fracture surface were the most important factors affecting seepage. Furthermore, Mandelbrot et al.[19] proposed a fractal geometry model, which has been widely used in the fractal modeling of irregular objects and surfaces.[20] Turkyilmazoglu[20−22] analyzed the momentum and thermal transport through a porous channel. He pointed out that compared with empty channels, the existence of porous metals in the channel with the surface slip leads to a better comprehensive performance of the system.

In terms of the movement mechanics of pulverized coal in coal seam fractures, Coste et al.[23] conducted a numerical simulation study of the mechanism of particle movement through an ideal flat plate model. It was found that there is a relatively high-pressure zone in the injection section. Coal particles near the high-pressure zone tend to have a large deformation, which tends to block the pore throat space. Fwa et al.[24] found that fine particles are more likely to be blocked by performing permeability tests on four different grades of rock samples. Additionally, Martin et al.[25] performed blocking tests on 10 common pores of different sizes and showed that the particle size distribution was closely related to the pore blocking, both before and after the permeability was closely related. Oseen et al.[26,27] modified the resistance expression of the Stokes formula by considering the effect of the inertial force term and theoretically corrected the Stokes formula. The modified result is closer to the experimental value than the Stokes formula. However, the error still exists at large Reynolds number. They also analyzed the settling process of particles in porous media and studied the settling, surface deposition, internal pore filling, and pore throat plugging processes of particles. Ganato et al.[28] calculated the theoretical equation of particle settlement and migration movement through the calculation model and obtained an analytical solution to the settlement problem. Liu, Clark, and Harkin[29,30] conducted a large number of coal particles settlement tests and recognized that the greater the proppant concentration, the more likely proppant settling occurs. Based on the settling and migration data of coal particles with different volume concentrations in transparent monolayer fracture channels, it was concluded that the greater the particle concentration, the more easily the particles would agglomerate into clumps and settle.

In terms of the simulation of pulverized coal migration, Kim et al.[31] developed the immersed boundary-finite volume method (IB-FVM), which introduces momentum forcing and mass sources to represent the submerged solid. This method uses a fixed grid to represent the fluid field instead of redistributing the fluid field, thus improving the computational speed and accuracy of the simulation. Mori and Peskin[32] developed an implicit second-order method to improve the stability of the immersion-boundary method. Bhardwaj and Mittal[33] used a combined immersed boundary-lattice Boltzmann method to study the deformation behavior of two-dimensional linear materials in fluids.

In this paper, the immersed boundary-lattice Boltzmann method is used to study the movement of pulverized coal particles in cracks under complex integration conditions. Compared with the traditional flow-particle coupling simulation method, the IB-LBM method could capture the fine seepage behavior in the micro-nanoscale seepage channel, which lays a foundation for the study of the flow particle interaction law in the seepage channel. Firstly, the coal seam fracture structure is modeled at the microscopic scale, and the Weierstrass−Mandelbrot (W−M) function is used to generate rough fractal curves of different sizes for several fractions. Secondly, the fluid flow velocity, permeability, and instantaneous flow velocity of pulverized coal particles carrying fluid under different fractal dimensions and driving pressures are calculated. Finally, the initiation and settling conditions of coal particles were investigated, and the effects of the migration state of pulverized coal particles and pulverized coal settling on the pore structure and permeability of coal seams were analyzed.

2. MODEL DESCRIPTION

2.1. Lattice-Boltzmann Method. LBM can be used to solve the isothermal compressive Navier−Stokes equations. Through Chapman−Enskog expansion,[34] the LB discretization method can be obtained and eventually converge to the incompressible N−S equations of the form,

$$\frac{\partial \boldsymbol{u}}{\partial t} + (\boldsymbol{u}\cdot\nabla)\boldsymbol{u} = -\frac{\nabla p}{\rho} + \nu\nabla^2\boldsymbol{u} + \boldsymbol{F} \tag{1}$$

$$\nabla\cdot\boldsymbol{u} = 0 \tag{2}$$

where $\boldsymbol{u}$ is the fluid velocity, t is the time, p is the pressure, ρ is the fluid density, and $\boldsymbol{F}$ is the forcing term. In the IB-LB method, the pushing or blocking effect of the solid boundary on the fluid is transformed into a force term, which is the most basic component of $\boldsymbol{F}$. The other part of $\boldsymbol{F}$ is the conservative force, e.g., gravity or a magnetic force.

In the LB method, the D2Q9 model is a common discrete format for solving eqs 1 and 2. In this model, the velocity is discretized microscopically into nine directions. The density distribution function is the only quantity of concern, and the discrete lattice-Boltzmann equation can be written as,

https://doi.org/10.1021/acsomega.3c02902
ACS Omega 2023, 8, 26369−26378

$$f_i(x + \boldsymbol{c}_i\delta t, t + \delta t) - f_i(x, t) = -\frac{1}{\tau}[f_i(x, t) - f_i^{eq}(x, t)] + F_i\delta t \quad (3)$$

where f_i is the density distribution function of the moving populations and $\boldsymbol{c}_i$ is the discrete velocity. In the D2Q9 model, $\boldsymbol{c}_i = \{c_{ix}, c_{iy}\}$ with $c_{ix} = (0,1,0,-1,0,1,-1,-1,1)$ and $c_{iy} = (0,0,1,0,-1,1,1,-1,-1)$. Here, τ is the dimensionless mean-relaxation coefficient and δt is the time step. The equilibrium distribution function $f_i^{eq}(x,t)$ is obtained by a Taylor-series expansion using the Maxwell−Boltzmann distribution function with velocity $\boldsymbol{u}$ up to the second order. It can be written as follows,

$$f_i^{eq}(\boldsymbol{x}, t) = \omega_i\rho\left(1 + \frac{\boldsymbol{c}_i\cdot\boldsymbol{u}}{c_s^2} + \frac{(\boldsymbol{c}_i\cdot\boldsymbol{u})^2}{2c_s^4} - \frac{\boldsymbol{u}^2}{2c_s^2}\right) \quad (4)$$

where ω_i is the weight coefficient associated with the velocity $\boldsymbol{c}_i$, and the non-dimensional lattice speed of sound is model-dependent. In the D2Q9 model, c_s usually equals $1/\sqrt{3}$ and $\omega_i = (4/9, 1/9, 1/9, 1/9, 1/9, 1/36, 1/36, 1/36, 1/36)$.

Applying the Chapman−Enskog multi-scale expansion method, the Navier−Stokes equations can be recovered using the LB equation with first-order time precision and second-order space precision. The density and local momentum are recovered by the summation and first-order moment of the density distribution function, respectively:

$$\rho = \sum_i f_i \quad (5)$$

$$\rho\boldsymbol{u} = \sum_i f_i\boldsymbol{c}_i \quad (6)$$

Conceptually, the LBM algorithm is implemented in two stages: collision and streaming. The collision step controls the relaxation toward equilibrium and the streaming step shifts the distribution functions to neighboring lattice cells,

$$\text{Collision: } f_i'(\boldsymbol{x}, t) = f_i(\boldsymbol{x}, t) - \frac{1}{\tau}[f_i(\boldsymbol{x}, t) - f_i^{eq}(\boldsymbol{x}, t)] + F_i(\boldsymbol{x}, t)\delta t \quad (7)$$

$$\text{Streaming: } f_i(\boldsymbol{x} + \boldsymbol{c}_i\delta t, t + \delta t) = f_i'(\boldsymbol{x}, t) \quad (8)$$

As mentioned above, $F_i(\boldsymbol{x}, t)$ is the discrete-force term. The discrete-force term is obtained as,

$$F_i(\boldsymbol{x}, t) = \left(1 - \frac{1}{2\tau}\right)\omega_i\left[\frac{\boldsymbol{c}_i - \boldsymbol{u}}{c_s^2} + \frac{\boldsymbol{c}_i\cdot\boldsymbol{u}}{c_s^2}\boldsymbol{c}_i\right]\cdot\boldsymbol{F}(\boldsymbol{x}, t) \quad (9)$$

However, the existence of an external force term changes the density and momentum, so it is necessary to correct the velocity,

$$\rho\boldsymbol{u} = \sum_i f_i\boldsymbol{c}_i + \frac{\delta t}{2}\boldsymbol{F} \quad (10)$$

Actually, there are many methods for dispersing force terms. However, the accuracy of this method is relatively highwith the ability to achieve second-order precision in space. In addition, the method's implementation is relatively simple.

2.2. Immersed Boundary-Lattice Boltzmann Method. In the numerical IBM scheme, the entire fluid domain is divided into a set of fixed lattice nodes, including the inner regions of the immersed bodies, e.g., particles. The model has two coordinate systems. The fluid nodes which do not move with the flow, are represented by Eulerian coordinates. On the other hand, the immersed boundary is discretized into a group of boundary points, which move under the action of the moving fluid and are represented by Lagrangian nodes. The immersed-boundary method (IBM), as applied to particulate flows, treats the particle boundary as deformable, but very stiff. A small distortion of the particle boundary will yield a force that tends to restore the particle to its original shape.

To model this description of a particle's physical surface, we consider a system with a particle with M discrete points. We assume that the particle's reference point is stationary, and all the boundary points lies on a circle. At time t, the center of the particle is located at position $\boldsymbol{x}_c(t) = \{x_c(t), y_c(t)\}$, and the instantaneous particle rotational matrix is $\boldsymbol{R}_i(t)$. The position of the reference point is calculated as follows,

$$\boldsymbol{x}_{ij}^r = \{x_{ij}^r, y_{ij}^r\} \quad (11)$$

$$x_{ij}^r(t) = x_c(t) + \boldsymbol{R}_i(t)\left[R\cos\left(\frac{j}{2\pi M}\right)\right] \quad (i = 1, 2..., n; j = 1, 2..., M) \quad (12)$$

$$y_{ij}^r(t) = y_c(t) + \boldsymbol{R}_i(t)\left[R\sin\left(\frac{j}{2\pi M}\right)\right] \quad (i = 1, 2..., n; j = 1, 2..., M) \quad (13)$$

where $x_c(t)$ and $y_c(t)$ are the center of the particle at time step t, which are calculated by velocity interpolation. The linear restoring force will determine when the reference point and the boundary point are not in the same position. We suppose that the particle deviation is $\boldsymbol{\xi}_{ij} = \boldsymbol{x}_{ij}(t) - \boldsymbol{x}_{ij}^r$. Subscript i indicates the ith particle, and subscript j indicates the jth discrete point.

3. RESULTS AND DISCUSSION

3.1. Rough Self-Affine Single Fracture Generation Method. Coal-based porous medium has the characteristics of cross-scale and anisotropy, making the quantitative characterization of pore structure of rock matrix and the law of fluid flow in porous medium a hot topic in geological research. The fractal dimension method is an efficient characterization technique to account for the spatial variability of fracture aperture (or irregular fracture-surface roughness), with widely exhibited self-affine fractal properties of natural fractures regardless of the host rock type, the fracture direction, and the fracture formation mechanism. Compared with the traditional JRC curve comparison method, the curves generated by the fractal method have better similarity to the natural fractures, and the fracture curvature can be controlled artificially.[35] In this study, a set of fractal structures with statistical characteristics is generated by using the self-affine fractal function of W−M.

Weierstrass−Mandelbrot function has been proved to have random self-affine property, and its function is continuous and non-differentiable everywhere. By dispersing the values of independent variables, a single fracture morphology curve with a finite lattice can be generated. Topography height coordinates are expressed by $Z(x)$. The expression is,

https://doi.org/10.1021/acsomega.3c02902
ACS Omega 2023, 8, 26369−26378

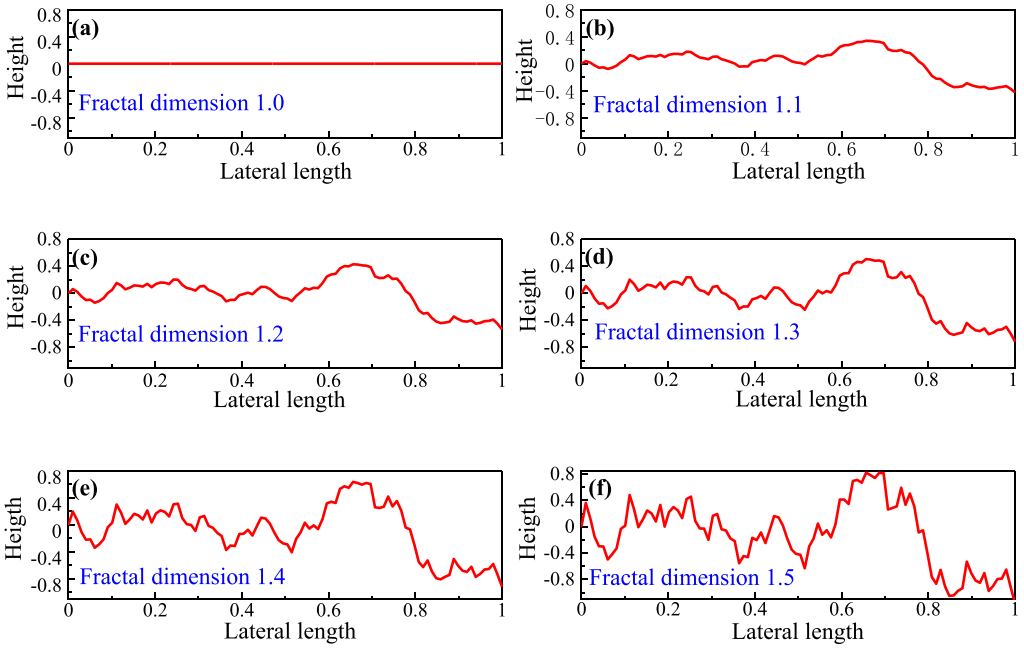

Figure 1. Two-dimensional fractal curves with fractal dimension of 1.0∼1.5. (a) Fractal dimension 1.0. (b) Fractal dimension 1.1. (c) Fractal dimension 1.2. (d) Fractal dimension 1.3. (e) Fractal dimension 1.4. and (f) Fractal dimension 1.5.

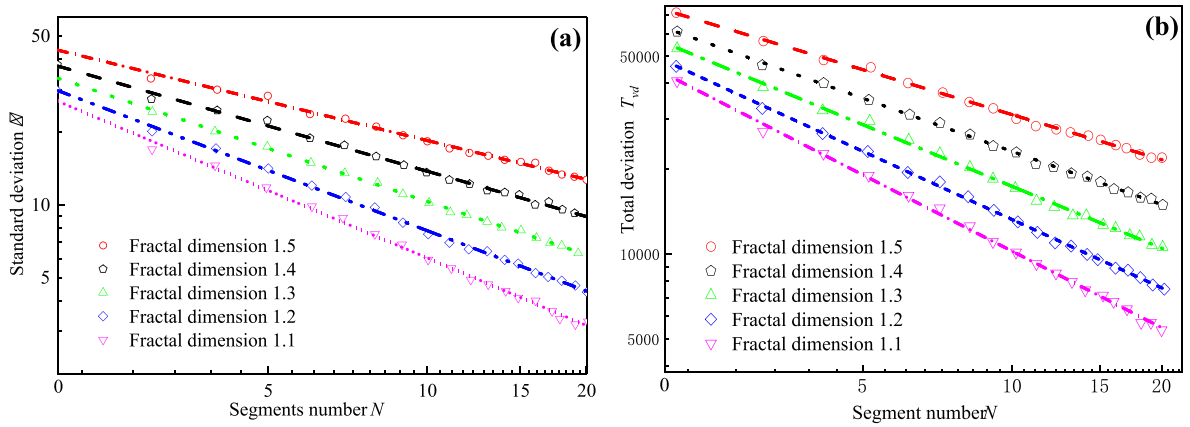

Figure 2. Linear regression analysis of the fractal curve standard deviation/total deviation with the number of segment number. (a) Standard deviation. (b) Total deviation.

$$Z(x) = G_{wm} \sum_{i=N_l}^{N_h} \gamma^{-i(2-D_f)} \cos\left(\frac{2\pi\gamma^i x}{L_s} + \phi_i\right) \quad (14)$$

where x is the transverse length; N_l and N_h are frequency control parameters, which control the probability of high frequency and low frequency occurrence of the fractal curve, In the simulation of this paper, the values of these two parameters are 1 and 1000, respectively. D_f is the self-affine fractal dimension of the generated curve, $D_f = 2 - H$ is generally taken, H is Hurst index, which can be obtained by statistical characteristics of fractures. G_{wm} is the height control factor, it is set to 4. γ is the sampling frequency factor, which is generally set to constant 1.5. L_s is the sample length, i.e., the number of grid points with discrete trending direction, in this case, L_s is set to 10,000. ϕ_i is the random factor of fracture curve, which ensures the randomness of fracture generation.

Figure 1 shows six groups of random fracture curves generated by W−M function. It can be seen from the figure that the fracture curve has random and self-affine characteristics. The curve shape becomes more tortuous as the fractal dimension of the fracture increases.. The W−M function can accurately characterize the shape of the natural fracture surface and optimize control parameters.

In order to verify the accuracy of the method, the linear regression characteristics of the fractal parameters of the curve with fractal dimension D = 1.0∼1.5 were analyzed in this paper. Firstly, the generated fractal curve is divided into several parts, expressed by N. With the change of N, the standard deviation σ and the vertical total deviation T_{vd} of the curve can be obtained for different number of sections. The change curves of standard deviation σ and total deviation T_{vd} can be drawn respectively, which can analyze the effectiveness of the six-component curve. Figure 2 shows the fitting relationship between the curve standard deviation, vertical total deviation and the number of curve segments, and there is a linear relationship between the two parameters and the logarithm of the number of segments N. The results show that the fractal

https://doi.org/10.1021/acsomega.3c02902
ACS Omega 2023, 8, 26369−26378

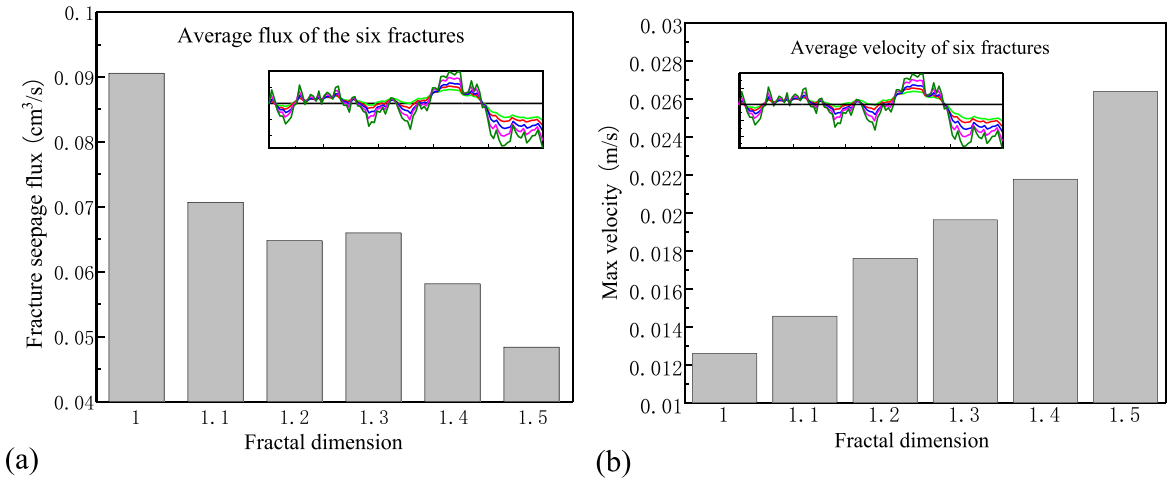

Figure 3. Variation of flow flux and velocity of fractures with different fractal dimensions. (a) Variation trend of fracture flow flux with fractal dimension. (b) Variation trend of maximum seepage velocity with fractal dimension.

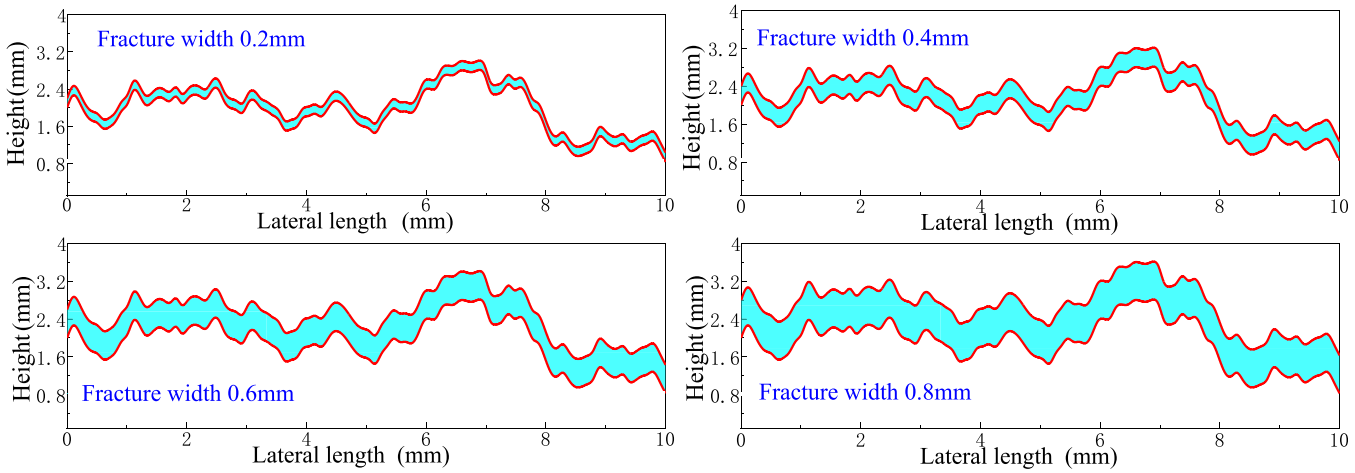

Figure 4. Fracture diagram with the fractal dimension D = 1.5 and the fracture width is 0.2, 0.4, 0.6 ,and 0.8 mm, respectively.

curve generation method retains the rough fractal characteristics of fractures.

3.2. Fluid Seepage in Single Fracture. In order to study the flow behavior of fluid in a single fractal fracture, this section simulates the flow of fluid under the influence of different roughness fracture morphology. Considering the complex fracture seepage process with different fractal dimensions, six fractal curves with different fractal dimensions are constructed, corresponding to six fracture structures with different roughness, as shown in Figure 3.

The channel length is set to 10 mm × 4 mm, and the fracture width is set to 0.4 mm. The lattice spacing of each grid point is 50 μm, and the number of grids is 200 × 80. The number of grids corresponding to the fracture width is 8 grids. The fluid density is 1000 kg/m^3, and the viscosity is 0.01 Pa s. The inlet and outlet are pressure boundary conditions, with a pressure difference of 1 kPa. The corresponding start-up pressure of the project is 5 MPa, which is similar to the drainage pressure of a 500 m deep coalbed methane well.

Numerically, when the fracture aperture is 0.4 mm and the fractal dimension is 1.1∼1.3, the fluid flow in the fracture has little difference. From the overall trend, the total fracture flow is negatively correlated with the fractal dimension. When the fractal dimension increases from 1.0 to 1.1, the flow flux decreases by 21%. When the fractal dimension is 1.2, the flow flux decreases by about 6%. When the fractal dimension is 1.3, the flow flux increases by about 2%. Therefore, the relationship between flow and fractal dimension is not strictly monotonically decreasing, and the inflection point of flow is the interval of fractal dimension 1.2∼1.3. This is because although the fractal dimension is a comprehensive consideration of fracture roughness, the fracture structure of coal matrix can affect seepage in many ways, and fractal dimension and effective fracture width jointly determine the seepage characteristics of fluid.

It can be seen from Figure 3 that the maximum velocity is positively correlated with the fractal dimension. With the same fracture width, the higher the fractal dimension, the more complex and narrow the effective fracture width.

Numerically, when the fracture aperture is 0.4 mm, the maximum fluid velocity is positively correlated with the fractal dimension. When the fractal dimension increases from 1.0 to 1.1, the maximum fracture flow velocity increases by 15%. When the fractal dimension 1.2, the flow velocity increases by 17% higher than that of 1.1. From the general trend observed, from fractal dimension 1.0 to fractal dimension 1.5, the fracture flow decreased by 120%, showing a steady and gradual decline. However, the maximum velocity is monotonically increasing

https://doi.org/10.1021/acsomega.3c02902
ACS Omega 2023, 8, 26369−26378

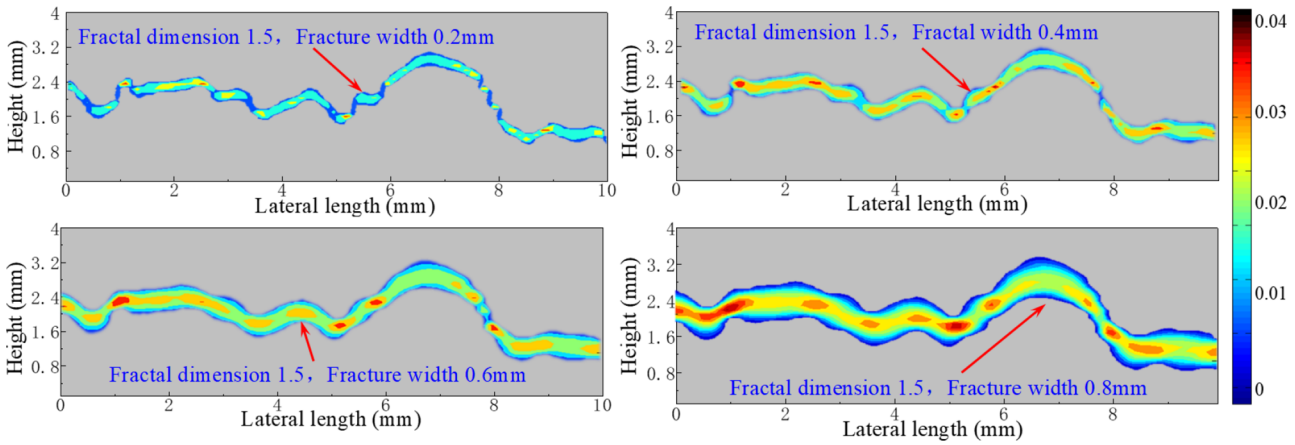

Figure 5. Seepage velocity of fractal dimension D = 1.5 and the fracture width is 0.2, 0.4, 0.6 ,and 0.8 mm, respectively.

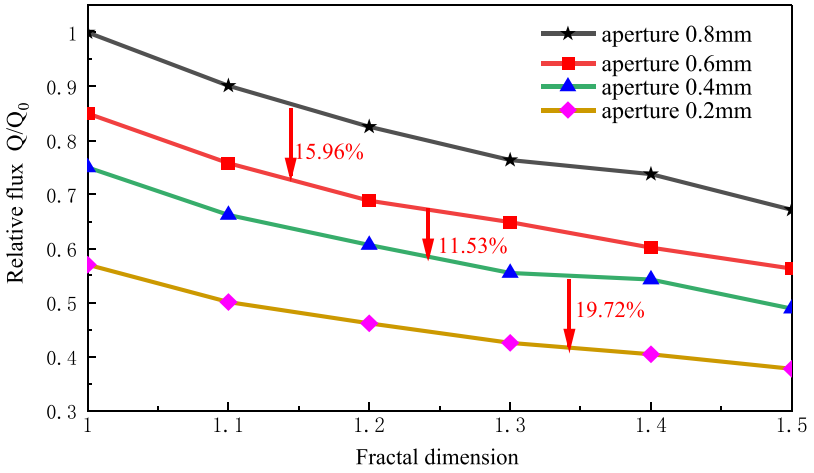

Figure 6. Flow variation of fracture fluid with fractal dimension at different apertures.

with the fractal dimension. The reason is that the increase of the fractal dimension reduces the effective width of the channel, which produces the slit effect and increases the fluid velocity.

At the same time, in order to study the change of flow rate in the fracture under the condition of the same fractal dimension but different aperture, four groups of single fracture curve models with different openings and six groups of different fractal dimensions were generated. In order to describe the fracture model intuitively, the fracture widths were set as 0.2, 0.4, 0.6 ,and 0.8 mm. The fracture width of each fractal dimension was set to four different clearance widths. Figure 4 shows the schematic diagram of four groups of fractures with aperture of 0.2, 0.4, 0.6 ,and 0.8 mm, respectively, when the fractal dimension is set to 1.5. Obviously, the fracture with larger aperture has larger cross section on the inclined section perpendicular to the interface, which makes the fluid in the wide channel have better passivity.

Figure 5 shows the contour map of fracture seepage velocity under different fracture degrees. It can be seen that under different apertures, the flow parameters of single fracture changes greatly, especially the flow velocity changes greatly. When the fracture aperture decreases, the maximum flow velocity in the fracture increases, but the total flow flux decreases.

Figure 6 shows the seepage condition of fractures and the statistical results of total flow under different fracture aperture. Under the condition of different fracture aperture, the relationship between seepage effect and apertures can be grasped as a whole by statistics of flow change in single fracture with different fractal dimensions.

According to the numerical analysis shown in Figure 6, when the fracture aperture is 0.8 mm, the seepage in the fracture passage reaches the maximum value. With the increase of fractal dimension, the seepage in the channel decreases. When the fracture aperture decreases to 0.6 mm, the average seepage flux decreases by 15.96%, indicating that the decrease in the fracture aperture leads to smaller fracture segments and reduced fluid permeability. When the fracture aperture decreases to 0.4 mm, the average fracture flow decreases by 11.53%. It can be seen from the relative flow trend diagram, with the increase of fracture fractal dimension, the influence of fracture opening gradually weakens. The decrease of fracture aperture and the increase of fractal dimension are the two main factors that weaken the co-directional relative flow of fractures.

The above studies have proved that the rough single fracture model can be constructed based on the complex curves with different fractal dimensions, and the lattice Boltzmann method has shown good applicability in simulating seepage in a single fracture. From the analysis of flow path and flow length, it is evident that tortuosity affects local pressure gradient of the flow field. Roughness is the main factor that changes the local flow pattern, and the difference of the roughness of the fracture leads to the change of the flow through the fracture.

https://doi.org/10.1021/acsomega.3c02902
ACS Omega 2023, 8, 26369−26378

3.3. Influence of Pulverized Coal Particle Size on Fluid Flow. In the process of coalbed methane drainage, a large number of coal particles are produced. Especially after the fracturing process, the coal seam is affected by the high pressure of water flow, and the coal matrix is affected by the impact of quartz sand and high-pressure water, forming a large number of fine coal particles. The particle size of these coal fine particles spans two orders of magnitude from 0.01 to 1 mm. In the process of drainage and production, different particle sizes of coal particles block the seepage channel formed by the original fracturing and hinder the effective exploitation of coalbed methane. In order to study the obstructing effect of coal fine particles on the passage in the process of migration, the immersed boundary-lattice Boltzmann method was used to simulate the fluid flow process of coal fine particles. The blocking effect of channel fractal dimension, channel width, particle size, number of coal fine particles, and particle size ratio of coal fine particles on flow was analyzed, respectively.

Figure 7 shows the schematic diagram of the ideal flow field with a bulge, while several representative geometric parameters

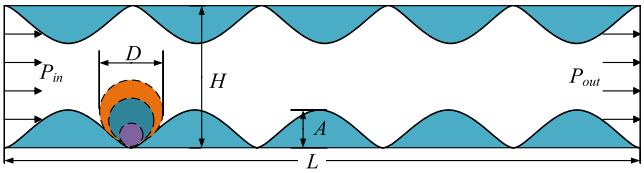

Figure 7. Schematic diagram of circular particle flow around an irregular wall channel.

of the fluid channel are given in the structural diagram. In order to study the influence law of the size of coal powder particles on the fluid percolation velocity in the channel, the height of the sinusoidal pipe wall in the channel is set to A. The fluid flow processes under the influence of three different particle sizes are compared and simulated in this case.

In the simulation model, the fluid density was set as 1000 kg/m^3, viscosity was 0.01 Pa s, particle density was set as 1250 kg/m^3, inlet and outlet were set as pressure boundary conditions, pressure difference was set as 0.01 kPa, and the upper and lower walls were set as static complete bounce-back boundary conditions to ensure that the velocity at the side wall was zero. The spacing of each grid point was 10 μm, the length of the whole flow field was 5 mm × 1 mm, the total grid number was 500 × 100, and the relaxation time in the simulation was set as 0.53.

In order to test the influence of particle size on fluid flow channel, the wall height A was set as 0.2 mm. The velocity distribution of the flow passage under four different conditions was analyzed. In the first case, the flow of fluid in a sinusoidal channel without particles was analyzed. The other three cases involved the study of a circular particle in the sinusoidal channel, with the diameters of the three circular particles being 0.12, 0.24, and 0.48 mm, respectively.

The simulated seepage channels in this paper conform to the fine microscopic seepage characteristics, and the seepage law satisfies Darcy's law of permeability. By converting the seepage velocity into microscopic permeability, the microscopic permeability change can be more intuitively reflected. The relationship between microscopic permeability and microscopic seepage velocity is,

$$K = \frac{\mu QL}{A\Delta p} = \frac{\mu L \int u_{in}(y)\mathrm{d}y}{A\Delta p} \tag{15}$$

where, Q is the total flow rate of seepage section, which can be obtained by numerical integration algorithm. L is the length of the path along which the fluid part flows, and A is the cross-sectional area of the fluid passage. Figure 8 shows the variation

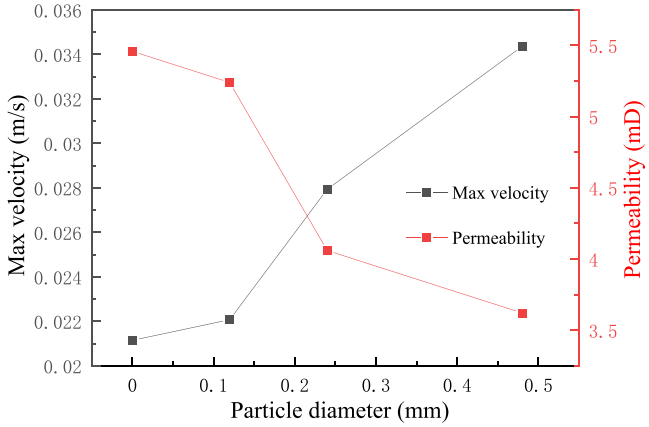

Figure 8. Maximum velocity and permeability of cross sections with different particle size.

of velocity and permeability with particle radius. The presence of large particles changes the main path of the flow field, thus changing the flux and permeability of the flow field. It is found that the permeability decreases with the increase of particle size.

It is worth mentioning that the permeability model described in this paper is the microscopic permeability model, which represents the seepage properties of microscopic porous media. On the other hand the permeability obtained through the experiment is generally macro permeability, and its calculation formula is,

$$k = -\frac{c\mu L}{AP_m\left(\frac{1}{V_1} + \frac{1}{V_2}\right)} \tag{16}$$

where V_1, V_2, L, A, P_m, and μ represent the upstream reservoir volume, downstream reservoir volume, shale sample length, shale sample crosssection area, mean pore pressure, and gas viscosity, respectively. The relationship between micro permeability K and macro permeability k was described in detail in the paper by Gao et al.[36]

3.4. Influence of Particle Number on Flow Passage. In order to study the effect of particle number on fluid movement in a complex fractal fracture, we selected a fracture with fractal dimension of 1.1 for the study and discussed the effect of pulverized coal particles number on fluid flow. Table 1 shows

Table 1. Cross-Section Flow and Permeability of Different Particle Sizes

particle number	maximum speed (m/s)	seepage flux (cm^3/s)	permeability (mD)	permeability reduction ratio (%)
0	0.03726	0.341	4.94	0
5	0.03245	0.329	4.77	3.44
10	0.03121	0.315	4.56	7.69
15	0.03065	0.296	4.29	13.16

https://doi.org/10.1021/acsomega.3c02902
ACS Omega 2023, 8, 26369−26378

the percolation velocity, percolation flux, and permeability in the complex curved channel with different number of particles. From the analysis of the results given in the table, it can be inferred that the seepage velocity decreases with the increase in the number of particles, and the seepage flux and permeability show similar results. Analyzing the reasons for this, the presence of particles reduces the cross-sectional area of fluid flow and hinders the passage of fluid. The flow creates a velocity crest area around the particles, but the effect is smaller than the decrease in permeability due to the reduction in the cross-sectional area of the fluid channel. The more coal particles in the channel, the larger the area of the channel occupied by the particles and the greater the blocking force on the fluid. As the number of particles increases, the flow channel area occupied by the particles increases and the blocking effect increases. To explain this problem from a microscopic point of view, an increase in the number of particles will lead to collisions between particles, seriously affecting the smooth flow of the fluid. The spinning force created by the particles also causes the formation of vortices, which slows down the fluid's speed. By analyzing the data in Table 1, it can also be found that more particles can significantly reduce the fluid flow and decrease the permeability of the fracture space. Meanwhile, the permeability reduction coefficient is significantly and positively correlated with the space occupied by the particles. The larger the space occupied by the particles, the greater the rate of permeability reduction. For instance, when the number of particles is doubled, the permeability in the passage decreases by about 3.5%.

3.5. Analysis of Particle Motion in Fracture with Different Fractal Dimensions. Considering the complex fracture seepage process with different fractal dimensions, six fractal curves with different fractal dimensions were constructed, corresponding to six fracture structures with different roughness. The fractal dimensions of the six different fractal curves were 1.0∼1.5. The channel length was set as 10 mm × 4 mm, and the fracture aperture was set as 1 mm. The spacing of each grid point was set as 50 μm, and the number of grids was 200 × 80. The fluid density was specified as 1000 kg/m^3 and the viscosity was set as 0.01 Pa s.

The results of seepage velocity, seepage flux, and permeability of the fluid in the channel containing pulverized coal particles with different fractal dimensions are shown in Table 2. Analyzing the data in the table, it can be concluded that with the increase of fractal dimension, the roughness of the fracture shows an increasing trend and the degree of curvature of the fracture channel is greater, which leads to the pulverized coal particles blocking the channel more easily. This leads to an exponential decrease of the permeability of the channel with the increase of the fractal dimension.

Table 2. Cross-Section Flow and Permeability of Different Fractal Dimensions

fractal dimension	maximum speed (m/s)	seepage flux (cm^3/s)	permeability (mD)	permeability reduction ratio (%)
1.0	0.03871	0.354	5.13	0
1.1	0.03251	0.309	4.32	15.79
1.2	0.02605	0.234	3.48	32.16
1.3	0.02433	0.206	3.31	35.48
1.4	0.02219	0.192	3.15	38.60
1.5	0.0209	0.188	3.06	40.35

Figure 9 shows the permeability variation curves for different fractal dimensions. Analyzing from the trend, the larger the fractal dimension of the fracture, the smaller the permeability of the channel. Numerically, the relationship between permeability and fractal dimension approximately conforms to a negative exponential relationship. The permeability of complex fractures is negatively correlated with the fractal dimension, while the permeability of granular fluids approximately satisfies the negative exponential law. The fractal dimension of the channel increases from 1.0 to 1.5, and the permeability of the channel decreases from 5.13 to 3.06 mD, with a 37% decrease in permeability.

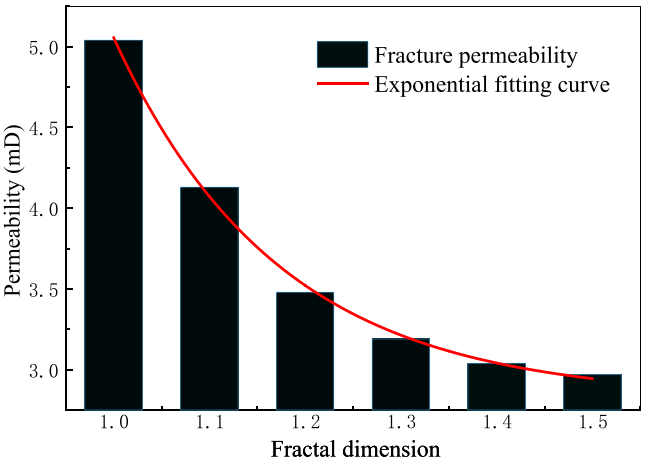

Figure 9. Fitting curve of permeability and fractal dimension.

3.6. Blocking Effect of Granular Composition on Fluid. In order to simulate the influence of particle size distribution on fluid seepage, the following four groups of particle size with different proportions were established, as shown in Figure 10. The cavity size of the four models is 8.1 mm × 8.1 mm, with a radius of 0.9 mm for large particles and 0.45 mm for small particles.

Figure 10 shows the contour map of velocity distribution when four particle size distributions are 1:0, 1:1, 1:2, and 1:4, respectively. With the increase in the number of small particles, that is, the ratio of large particles to small particles, the fluid seepage channel becomes more complicated and the seepage path becomes more tortuous. As a result, the fluid seepage velocity increases significantly, but the overall permeability decreases. From the perspective of the effective length of the channel, in the coal seam channel with better grain distribution, the fluid needs to pass through a longer path, so the effective permeability decreases. Increasing the particle size ratio makes the fluid path more dispersed, which is not enough to form a large main seepage path and reduce permeability.

Figure 11 shows the variation curves of maximum flow velocity and permeability in the channel under different particle gradation ratios. It is found that when the particle gradation degree is high, and the medium space is evenly occupied by the interlacing of large and small particles, the fluid velocity increases at the local location. When the ratio of large particle size to small particle size increases from 1:0 to 1:4, the permeability of pore space decreases from 5.32 to 4.01 mD, resulting in a permeability reduction rate of 24.63%. The maximum flow velocity in the channel increased from 0.023 to 0.040 m/s, with an increase of 73.91%. The above analysis

https://doi.org/10.1021/acsomega.3c02902
ACS Omega 2023, 8, 26369−26378

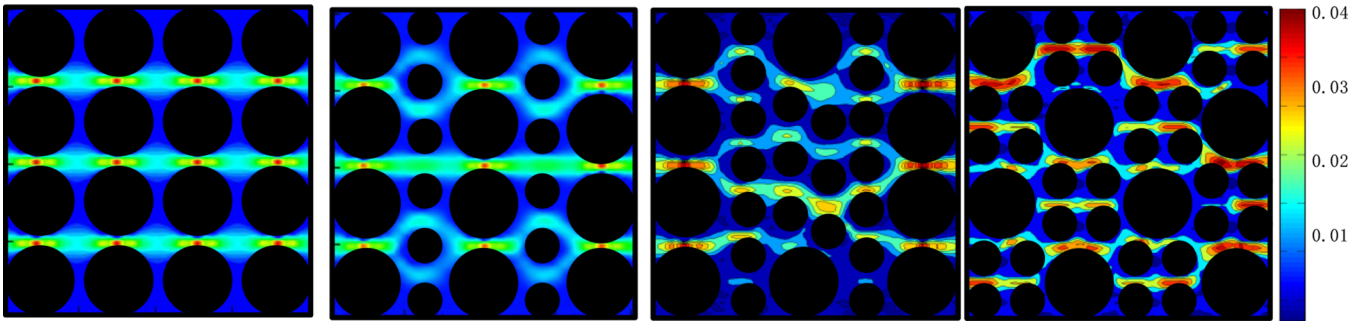

Figure 10. Contour map of flow velocity of circular particles in a square cavity.

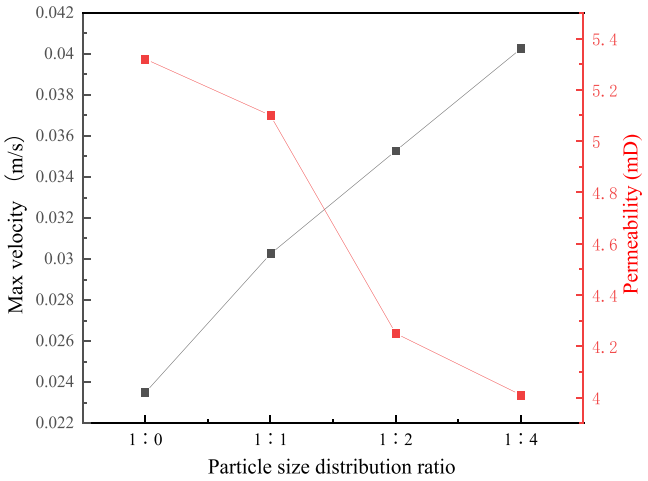

Figure 11. Maximum velocity and permeability of cross sections with different particle composition.

shows that the increase of particle gradation degree will reduce the permeability in the channel, and the coal particle pile with better particle gradation degree will hinder the transportation of formation fluid to a greater extent. In actual production process, effective measures to avoid pulverized coal particles particle size mutual accumulation, is to control the formation of fluid production rate, the reasonable layout of the mining system, control water rate that can carry small particle size of pulverized coal particles conveying to the wellbore, make the part of the pulverized coal particles shaft discharge, while another part of pulverized coal particles can be deposited at the bottom of the pocket, reducing the particle size of pulverized coal particles filling each other on the negative impact of high rank.

4. CONCLUSIONS

The study of this paper summarizes the plugging phenomenon of pulverized coal particles in coalbed methane fractures and explores the plugging law of pulverized coal particles, which can provide data basis for the pressure control of CBM well drainage. In summary, the following main conclusions are drawn in this paper:

(1) The immersed boundary-lattice Boltzmann numerical method has accurate numerical accuracy in simulating the fluid−structure interaction problem. After verifying the accuracy of the method, a simulation study was done for the fracture aperture on fluid seepage, and the results show that the seepage effects of fracture networks with different pore diameters were significantly different.

(2) The blocking effect of pulverized coal particles with different particle sizes on seepage channel was investigated. The results showed that when the particle size is smaller than the bump height of the channel, there is almost no significant difference. When the particle size is larger than the projection height of the fissure, the larger the particle size is, the greater the obstruction effect on the channel.

(3) The effect of particle number on percolation flow was investigated. The results show that the presence of particles reduces the cross-sectional area of fluid flow and impedes the passage of fluid. The increase in fluid velocity around the particle is not as significant as the decrease in permeability caused by the decrease in the cross-sectional area of the fluid channel. As the number of particles increases, the blocking effect increases and the area of the fluid channel occupied by the particles increases.

(4) The blocking effect of coal dust particles with different particle gradations on the flow channel was compared. The results show that the maximum percolation velocity increases significantly and the overall permeability decreases with the increase of the number of small particles.

AUTHOR INFORMATION

Corresponding Author

Songlei Tang − *Xi'an Modern Chemistry Research Institution, Xi'an 710065, China;* orcid.org/0000-0002-6263-7205; Email: tangsonglei@foxmail.com

Authors

Qiang Liu − *Xi'an Modern Chemistry Research Institution, Xi'an 710065, China*

Hong Tang − *Xi'an Modern Chemistry Research Institution, Xi'an 710065, China*

Feng Yang − *Xi'an Modern Chemistry Research Institution, Xi'an 710065, China*

Complete contact information is available at: https://pubs.acs.org/10.1021/acsomega.3c02902

Notes

The authors declare no competing financial interest.

ACKNOWLEDGMENTS

This project is granted by the National Natural Science Foundation of China (41472130).

https://doi.org/10.1021/acsomega.3c02902
ACS Omega 2023, 8, 26369−26378

REFERENCES

(1) Xue, S.; Zheng, C.; Kizil, M.; et al. Coal permeability models for enhancing performance of clean gas drainage: A review. *J. Pet. Sci. Eng.* **2021**, *199*, No. 108283.

(2) Moore, T. A. Coalbed methane: A review. *Int. J. Coal Geol.* **2012**, *101*, 36−81.

(3) Shi, J.; Wu, J.; Fang, Y.; Lu, J.; Hou, C.; Li, X.; Zhang, S.; Xiong, X. A new coal reservoir permeability model considering the influence of pulverized coal particles blockage and its application. *Nat. Gas Ind. B* **2021**, *8*, 67−78.

(4) Zhang, F. N.; Qi, Y. G.; Xu, C. C.; et al. Analysis of the impact of gas production channel for coalbed methane well by pulverized coal particles. *J. China Univ. Min. Technol.* **2013**, *42*, 428−435.

(5) Tan, P.; Jin, Y.; Yuan, L.; Xiong, Z.-Y.; Hou, B.; Chen, M.; Wan, L.-M. Understanding hydraulic fracture propagation behavior in tight sandstone−coal interbedded formations: an experimentalinvestigation. *Pet. Sci.* **2019**, *16*, 148−160.

(6) Li, H.; Lau, H. C.; Huang, S. Coalbed methane development in China: Engineering challenges and opportunities. *J. Pet. Sci. Eng.* **2018**, 166.

(7) Thakur, P. Coalbed Methane Production From Deep Coal Reservoirs. *Advanced Reservoir and Production Engineering for Coal Bed Methane* 2017, 171 −190.

(8) Han, G.; Ling, K.; Wu, H.; Gao, F.; Zhu, F.; Zhang, M. An experimental study of coal-fines migration in Coalbed-methane production wells. *J. Nat. Gas Sci. Eng.* **2015**, *26*, 1542−1548.

(9) Bedrikovetsky, P.; Zeinijahromi, A.; Siqueira, F. D.; et al. Particle Detachment Under Velocity Alternation During Suspension Transport in Porous Media. *Transp. Porous Media* **2012**, *91*, 173−197.

(10) You, Z.; Bedrikovetsky, P.; Badalyan, A.; et al. Particle mobilization in porous media: Temperature effects on competing electrostatic and drag forces. *Geophys. Res. Lett.* **2015**, *42*, 2852−2860.

(11) Bedrikovetsky, P.; Caruso, N. Analytical Model for Fines Migration During Water Injection. *Transp. Porous Media* **2014**, *101*, 161−189.

(12) Wei, Y.; Chao, L. I.; Cao, D. et al. New Progress on the Pulverized coal particles Affecting the Development of Coalbed Methane. *Acta Geol. Sin. (Engl. Ed)* 2018, *92* (5), 2060−2062, DOI: 10.1111/1755-6724.13708.

(13) Wei, Y.; Zhang, A.; Cao, D.; et al. Characteristics of pulverized coal particles during coalbed methane drainage in Linfen block. *Coal Geol. Explor.* **2016**, *44*, 30−35.

(14) Xu, B.; Li, X.; Haghighi, M.; Du, X.; Yang, X.; Chen, D.; Zhai, Y. An analytical model for desorption area in coal-bed methane production wells. *Fuel* **2013**, *106*, 766−772.

(15) Payatakes, A. C.; Tien, C.; Turian, R. M. A new model for granular porous media: Part I. Model formulation. *AIChE J.* **1973**, *19*, 58−67.

(16) Reddi, L. N.; Bonala, M. V. S. Analytical Solution for Fine Particle Accumulation in Soil Filters. *J. Geotech. Geoenviron. Eng.* **1997**, *123*, 1143−1152.

(17) Happel, J.; Brenner, H. *Low Reynolds number hydrodynamics: With special applications to particulate media*; Springer Science and Business Media 2012, *1*, 159 −234.

(18) Bandis, S.; et al. Experimental studies of scale effects on the shear behaviour of rock joints. *Int. J. Rock Mech. Min. Sci. Geomech. Abstr.* **1981**, *18*, 1−21.

(19) Mandelbrot, B. B.; Passoja, D. E.; Paullay, A. J. Fractal Character of Fracture Surfaces of Metal. *Nature* **1984**, *308*, 721−722.

(20) Turkyilmazoglu, M. Velocity Slip and Entropy Generation Phenomena in Thermal Transport Through Metallic Porous Channel. *J. Non-Equilib. Thermodyn.* **2020**, *45*, 247−256.

(21) Turkyilmazoglu, M. Accelerating the convergence of Adomian decomposition method (ADM). *J. Comput. Sci.* **2019**, *31*, 54−59.

(22) Turkyilmazoglu, M. Bodewadt flow and heat transfer of dusty fluid with Navier slip. *Arch. Mech.* **2022**, *74*, 157−172.

(23) Coste, J.P.; Liu, Y.; Bai, B., et al. In-depth fluid diversion by pregelled particales. Laboratory study and pilot testing. *Prsented at SPE/DOE Improved Oil Recovery Symposium, 3−5 April, Tulsa, Oklahoma. SPE-59362-MS.*

(24) Fwa, T.; Tan, S.; Guwe, Y. Laboratory Evaluation of Clogging Potential of Porous Asphalt Mixtures. *Transp. Res. Rec.* **1999**, *1681*, 43−49.

(25) Martin, W. D.; Putman, B. J.; Neptune, A. I. Influence of aggregate gradation on clogging characteristics of porous asphalt mixtures. *J. Mater. Civ. Eng.* **2014**, *26*, 1−7.

(26) Ghorbani, Y.; Mainza, A. N.; Petersen, J.; et al. Investigation of particles with high crack density produced by HPGR and its effect on the redistribution of the particle size fraction in heaps. *Miner. Eng.* **2013**, *43-44*, 44−51.

(27) Ding, Y. D.; Langouët, H.; Jeannin, L. Simulation of Fracturing Induced Formation Damage and Gas Production. *SPE Middle East Unconventional Gas Conference and Exhibition, 23−25 January*; UAE, Society of Petroleum Engineers: Abu Dhabi, 2012, 101−146.

(28) Berkowitz, B.; Cortis, A.; Dentz, M.; Scher, H. Modeling non-Fickian transport in geological formations as a continuous time random walk. *Rev. Geophys.* **2006**, *44*, 466−480.

(29) Zheng, X.-L.; Shan, B.-B.; Chen, L.; Sun, Y.-W.; Zhang, S.-H. Attachment-detachment dynamics of suspended particle inporous media: Experiment and modeling. *J. Hydrol.* **2014**, *511*, 199−204.

(30) Barth, T.; Reiche, M.; Banowski, M.; Oppermann, M.; Hampel, U. Experimental investigation of multilayer particle deposition and resuspension between periodic steps in turbulent flows. *J. Aerosol Sci.* **2013**, *64*, 111−124.

(31) Kim, J.; Kim, D.; Choi, H. An Immersed-Boundary Finite-Volume Method for Simulations of Flow in Complex Geometries. *Comput. Phys.* **2001**, *171*, 132−150.

(32) Mori, Y.; Fishman, G. I.; Peskin, C. S. Ephaptic conduction in a cardiac strand model with 3D electrodiffusion. *Proc. Natl. Acad. Sci. U. S. A.* **2008**, *105*, 6463−6468.

(33) Bhardwaj, R.; Mittal, R. Benchmarking a Coupled Immersed-Boundary-Finite-Element Solver for Large-Scale Flow-Induced Deformation. *AIAA J.* **2012**, *50*, 1638−1642.

(34) Liu, S.; Tang, S.; Lv, M.; et al. Simulating particle sedimentation in a flowing fluid using an immersed boundary−lattice Boltzmann method. *Int. J. Comput. Fluid Dyn.* **2020**, *34*, 39−49.

(35) Chang, C.; Ju, Y.; Xie, H.; et al. Non-Darcy interfacial dynamics of air-water two-phase flow in rough fractures under drainage conditions. *Sci. Rep.* **2017**, *7*, 4570.

(36) Gao, Q.; Han, S. C.; Cheng, Y.; et al. Apparent permeability model for gas transport through micropores and microfractures in shale reservoirs. *Fuel* **2021**, *285*, No. 119086.

https://doi.org/10.1021/acsomega.3c02902
ACS Omega 2023, 8, 26369−26378